Journal of Materials Chemistry A

Accepted Manuscript

ROYAL SOCIETY OF CHEMISTRY

www.rsc.org/materialsA

Journal of Materials Chemistry A

COMMUNICATION

Hydrogen Evolution Reaction in Acidic Media on Single-Crystalline Titanium Nitride Nanowires as an Efficient Non-Noble Metal Electrocatalyst

Received 00th January 20xx,
Accepted 00th January 20xx

DOI: 10.1039/x0xx00000x

www.rsc.org/

Yujie Han[1,†], Xin Yue[1,†], Yanshuo Jin[1], Xiangdong Huang[2] and Pei Kang Shen[1,*]

Single-crystalline titanium nitride nanowires (TiN NWs) have been directly synthesized by a novel chemical vapor deposition (CVD) method and used as efficient catalysts for hydrogen evolution reaction (HER) for the first time. Electrochemical test reveals good HER performance of TiN NWs, with low overpotential of 92 mV at 1 mA cm^{-2} and a Tafel slope of 54 mV dec^{-1}. After 20000 cycles and 100 h durability test as well in acidic media, the current density remains nearly unchanged, revealing superior chemical stability of as synthesized TiN NWs for HER.

Global utilization of fossil fuels for energy needs is rapidly resulting in critical environmental problems throughout the world. Hydrogen is a promising future energy carriers to solve the issue, while water electrolysis is one of the most important ways for hydrogen production.[1,2] Thus developing highly efficient, stable and environmentally friendly catalysts for water electrolysis is very important.

Pt-based catalysts has superior catalytic properties for hydrogen evolution reaction (HER) in water electrolysis, however, their high cost and scarcity limit their use in practical applications. During the past several decades, scientists have made much effort in developing efficient non-noble metal electrocatalysts with the aim of providing cost-competitive hydrogen.[3] Among them, transition metal nitrides are considered to have similar properties to noble metals due to their unique electron structures, which attract much attention.[4] Many transition metal nitrides owning good HER properties have been developed in recent years, such as WN, MoN, $NiMoN_x$, $Co_{0.6}Mo_{1.4}N_2$ and so on.[5-8]

Titanium nitride (TiN) is also one of the promising catalysts for HER, due to its superior electrical conductivity,[9, 10] and excellent corrosion resistance in aqueous solutions.[4] However, previous work revealed that the commercial bulk TiN particles showed poor HER activity with high overpotential due to its low surface area, low crystallinity and irregular morphology, while few work has been down to improve TiN's HER performance. Constructing a new morphology with high surface area and fast electron transport rate is helpful to improve the activity of the catalyst, and TiN nanowires with 1D morphology have been used in many fields due to its superior properties.[9, 11-14] However, most of the TiN nanowires was synthesized indirectly by nitridizing TiO_2 nanowires, which brings the problem of incomplete nitridation, leading to poor conductivity.

Herein, we report a novel CVD method to directly synthesis single-crystalline TiN nanowires, the TiN NWs was grown on a graphite bar substrate in N_2 atmosphere. Anion exchange resin D301 exchanged with $Co(NO_2)_6^{3-}$ ions and TiF_6^{2-} ions (D301-Co-Ti) was used as precursor, acting both as Ti source and catalyst for the growth of TiN NWs. As synthesized TiN NWs is single-crystalline along the whole length with uniform 1D morphology, which could offer higher conductivity and constructing a fast electron transport network, thus demonstrate good performance and superior electrochemical stabilities in HER reaction.

Scheme 1 illustrates the process to synthesize TiN NWs. As a precursor, the anion exchange resin powders were substantially exchanged with $Co(NO_2)_6^{3-}$ ions and TiF_6^{2-} ions. A graphite bar substrate was then put on top of the as prepared precursor powders and annealed at 1200 ^{o}C for 2 h in N_2 atmosphere to grow TiN NWs. A layer of golden brown TiN NWs will grow on the top surface of the substrate. The as grown TiN NWs was then collected from the substrate and washed with HCl and deionized (DI) water to remove the impurities (See Electronic Supplementary Information(ESI) for the details of the synthesis scheme).

[1] State Key Laboratory of Optoelectronic Materials and Technologies, and Guangdong Province Key Laboratory of Low-carbon Chemistry & Energy Conservation, School of Physics and Engineering, Sun Yat-sen University, Guangzhou, 510275, PR China
*Correspondence to stsspk@mail.sysu.edu.cn;
[2] Guangzhou Automobile Group Co., Ltd., Guangzhou, 510640, PR China.
†The authors contributed equally.

Electronic Supplementary Information (ESI) available: Additional data for the characterization and experiment details. See DOI: 10.1039/x0xx00000x

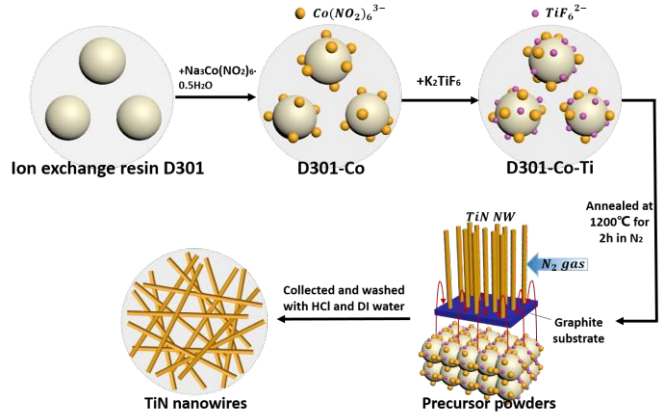

Scheme 1. Schematic illustration of TiN NWs synthesis.

A series of comparison experiments has been down to understand the growth mechanism of the TiN NWs. When annealed in Ar atmosphere instead of N_2, TiC/C instead of TiN/C was synthesized in the precursor powder, revealing that N_2 act as the nitrogen source (Figure S6). D301-Co-Ti precursor plays an important role in the growth of TiN NWs, on the one hand, anion exchange resin will act as the carbon reducer at high temperature similar to the well-known carbon-thermal reduction synthesis method of TiN,[15] on the other hand, $Co(NO_2)_6^{3-}$ ions will reduced by the carbon into elemental Co and further act as a catalyst, as previously reported in the literature[16], and further confirmed in Figure S6(more details was discussed in ESI). The growth of TiN nanowires could be understood by combination of the well-known vapor–liquid–solid (VLS) and vapor–solid (VS) growth mechanism.[17,18] In the initial growth stage of TiN nanowires, the gaseous Ti elements and N_2 diffused onto the surface of the liquid Co catalyst droplet to form Co–Ti–N alloy droplet. When super saturation was reached due to the continual supply of Ti atoms evaporated from the precursor powders and N_2 gas, TiN nanowires were formed with the assist of the Co-Ti-N alloy dorplet. In addition, the Co in Co–Ti–N droplet might be gradually consumed and took away by the flowing gas. Hence in the final product, Co catalyst particles could not be observed at the ends of TiN nanowires. After the initial VLS growth of the TiN nanowires, it is also possible for the further growth through direct VS manner from the emitted Ti element and N_2, with continuing Ti element provided from the precursor powders and adequate N_2 gas supply, ultralong single-crystalline TiN NWs were gradually formed, which was in accordance with the growth mechanism of TiN nanowires previously studied by Hu *et al*.[12]

Figure 1a and 1b show typical SEM images of the TiN NWs grown at 1200 °C for 2 h. The scanning electron microscopy (SEM) image demonstrated the uniform 1D morphologies of the as synthesized TiN NWs. TiN nanowires reached an ultralong average length up to 100 μm and 330 nm in width, significantly differing from the morphology of larger and irregular commercial bulk TiN particles (Figure S1). The SEM images of TiN

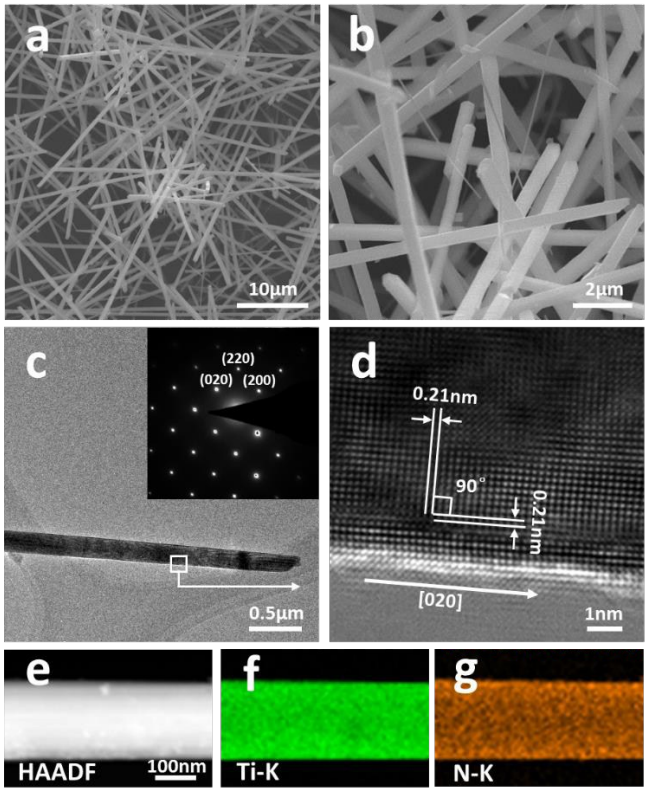

Fig.1 (a,b) SEM images of as synthesized TiN NWs. (c,d) TEM images of one TiN nanowire and its corresponding SAED pattern and HRTEM images. (e-g) STEM-HAADF images and element mapping images of TiN nanowire.

NWs grown at 1300°C and 1400 °C for 2 h is also shown in Figure S9. The ultralong TiN NWs gathered together to form a network like morphology which could offer high surface area, high charge transfer rate and good electrical conductivity. The nanowires are single-crystalline, as evidenced by the SAED pattern of a nanowire examined along the [00$\bar{2}$] zone axis (Figure 1c), and the electron diffraction spots are corresponding to the (020), (220), (200) facets of TiN, respectively. Compared with the polycrystalline TiN reported in the literature[19, 20], the as prepared TiN nanowires suggests an attractive single-crystalline nature and high crystallinity, which can result in excellent electrical conductivity[21], thus be beneficial for the electrocatalytic reactions in our experiments. Figure 1d shows the HRTEM examination of one individual nanowire, the lattice fringes with interplanar spacing $d_{(200)}=d_{(020)}$=0.21nm are imaged and the interplanar angle is measured to be 90°, which are consistent with the XRD data. The [00$\bar{2}$] axis is perpendicular to the nanowire side walls, revealing that the nanowires grow along the [020] direction. Figure 1e-g show the HAADF STEM image and corresponding elemental mapping analysis of a randomly selected area of TiN nanowire. N detections emerge at the same position where Ti is also detected, Ti and N elements are uniformly distributed in the nanowire.

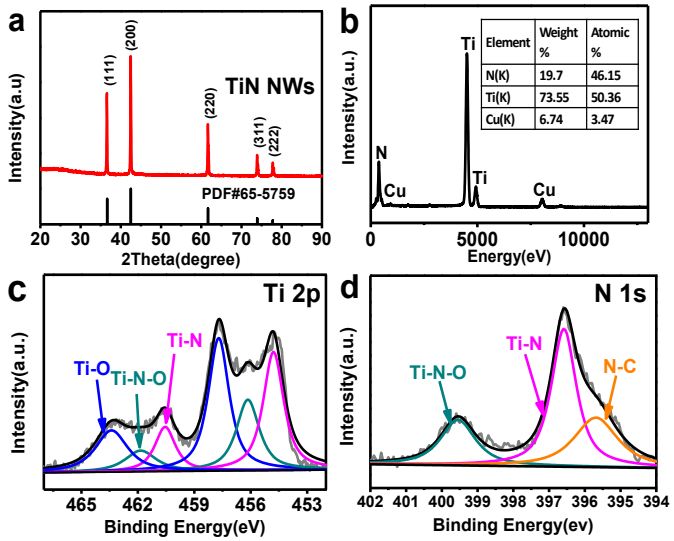

Fig.2 (a) XRD pattern of TiN NWs.(b)EDX spectrum of TiN NWs (c) Ti 2p and (d)N 1s XPS spectra of TiN NWs.

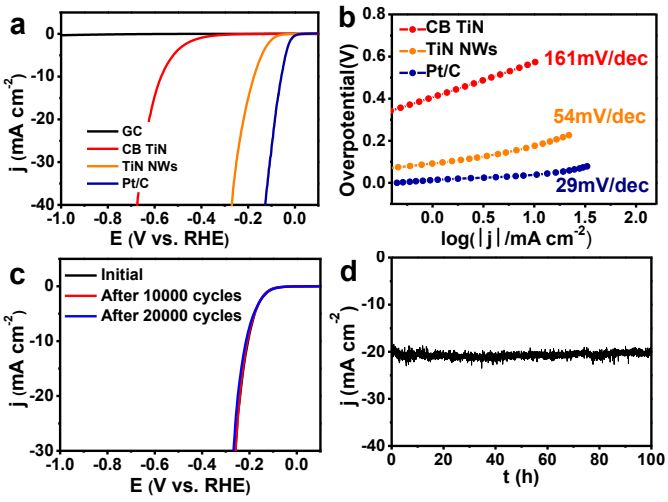

Fig.3 (a) Polarization curves (after IR correction) for the TiN NWs electrodes in 1 M $HClO_4$, along with CB TiN, commercial Pt/C, and bare glassy carbon(GC) electrode in 1M $HClO_4$, for comparison, (b) corresponding Tafel plots for the TiN NW, CB TiN and Pt/C electrodes, (c) stability tests of TiN NWs catalyst through potential cycling, in which the initial polarization curve as well as polarization curves after both 10000 and 20000 potential cycles are displayed and (d) time dependence of cathodic current density during electrolysis over 100 h at fixed potential of -240 mV (after IR correction).

Figure 2a shows the XRD pattern of the TiN NWs and the model structure of the TiN. The main diffraction peaks at 2θ=36.5°, 42.5°, 61.7°, 73.9° and 77.8° are assigned to (111), (200), (220), (311), and (222) facets of TiN (PDF #65-5759), respectively. No other peaks were observed in the pattern, indicating that highly pure TiN nanowires were produced. EDX was further taken to examine the chemical stoichiometry of the TiN nanowires (Figure 2b). The atomic ratio of N to Ti is ~1:1, which is in accordance with the theoretical value of titanium nitride, and the detected Cu element is from the copper grid.

XPS spectroscopy was further used to confirm the surface chemical composition and oxidation state of products (Figure 2c and 2d). The Ti 2p spectrum of the TiN exhibits multiple peaks, which can be assigned to be Ti–N ($2p_{3/2}$= 454.77 eV and $2p_{1/2}$= 460.53 eV), Ti–N–O ($2p_{3/2}$= 456.14 eV and $2p_{1/2}$= 461.90 eV), and Ti–O ($2p_{3/2}$ = 457.80 eV and $2p_{1/2}$ = 463.56 eV), which is consistent with typical values reported for TiN.[22,23] The N 1s spectra show three contributions situated at 396.6 eV, 395.6 eV and 399.5 eV. The first one at 396.6 eV which is also the main one is attributed to Ti-N bond. The one at 395.6 eV could be due to N-C bond, which might come from the surface carbon-nitride compounds. The last one at 399.5 eV is assigned to be Ti-N-O bond,[22] which is in accordance with the Ti 2p spectra. These results reveal that the surface of as synthesized TiN NWs are composed of Ti–N–O, Ti–N, and Ti–O chemical states.

The electrocatalytic HER activity of the TiN NWs sample was investigated by depositing it on a glassy carbon(GC) electrode with an optimal catalyst loading of 0.51 mg cm^{-2}, and the effect of the loading amount for TiN NWs electrode performance was investigated in Figure S7. The experiment was conducted in 1 M $HClO_4$ solution at 25 °C using a three-electrode setup. For comparison, commercial bulky TiN (CB TiN) was also tested by depositing it on a carbon electrode with the same catalyst loading amount, as well as bare glassy carbon electrode(see ESI for the details of the electrode preparation). Figure 3a shows the polarization curves of each individual electrode(the corresponding CV curves was showed in Figure S8). For the TiN NWs, the catalytic current was observed at a low onset overpotential of approximately 92 mV (*vs.* RHE) at 1 mA cm^{-2}, above which the current density increases rapidly at more negative potentials with substantial current density of approximately 40 mA cm^{-2} at an overpotential of 270 mV. Such electrocatalytic activity is one of the best data reported for transition metal nitride catalysts up to date(Table S1), and also comparable to some of the best non-noble catalyst reported in recent years[8, 24-28]. In contrast, a CB TiN electrode showed much less HER activity, with a much higher onset overpotential of about 405 mV at 1 mA cm^{-2}, 313 mV higher than that of the TiN NWs. Commercial bulky TiN particles had smaller surface areas and exhibited lower catalytic activities, indicating that the surface area is a crucial structural parameter dominating the HER, as reported widely in the literature.[3] Additionally,we also investigated the effect of the growth temperature to the HER peformance of TiN NWs (Figure S10), the TiN NWs synthesised at 1200 °C with smallest average diameter and longest average length shows best peformance towards HER (more details discussed in ESI). We attribute the significantly improved catalytic activity of our TiN NWs catalyst in HER to the specific network like structure formed by as synthesized ultralong single-crystalline TiN, contributing to large surface

areas, good conductivity and fast charge transfer rate of the electrode.

Figure 3b shows the corresponding Tafel plots for TiN NWs, CB TiN and Pt/C. The Pt/C electrode exhibited a Tafel slope of 29 mV/decade and an exchange current density of 5.7 $\times 10^{-1}$ mA cm^{-2}. Both parameters are consistent with the high activity and the known mechanism of the HER on Pt/C.[29, 30] Bulk TiN electrode, was not significantly active for the HER, displaying an exchange current density of 3.16×10^{-3} mA cm^{-2} and a Tafel slope of 161 mV dec^{-1}. Tafel analysis of the TiN NWs indicated an exchange current density of 3.16×10^{-2} mA cm^{-2} and a Tafel slope of 54 mV dec^{-1}. Typically, the exchange current density is expected to be proportional to catalytic active surface area. An alternative approach to estimate the effective surface area is to measure the capacitance of the double layer at the solid-liquid interface with cyclic voltammetry,[32] as shown in Figure S11, the capacitance of CB TiN electrode is 0.37mF cm^{-2}, while the capacitance of TiN NWs electrode is 4.52 mF cm^{-2}, about 11 times higher than that of the CB TiN electrode. The Tafel slope of the TiN NWs do not match the expected Tafel slopes of 29, 42, and 118 mV dec^{-1}, each of which correlate with a different rate-determining step of the HER.[31] However, the 54 mV/decade Tafel slope falls in the range of 42–118 mV dec^{-1}, suggesting that the HER taking place on the TiN NWs surface would follow a Volmer–Heyrovsky mechanism, and the electrochemical desorption step of hydrogen is rate-limiting.[33, 34]

Aside from the requirement for high activity, good durability is also an important factor for electrocatalysts. To investigate the durability under electrocatalytic operation, the TiN NWs catalyst was continuously cycled for a total of more than 20000 cycles in 1 M $HClO_4$ (Figure 3c). The current density of TiN NWs remained nearly unchanged after 10000 cycles, and slightly decreased to about 90% after 20000 cycles, indicating the excellent electrochemical stability of the TiN NWs. Furthermore, the practical operation of the catalyst is examined by electrolysis at a fixed potential for an extended period of time (Figure 3d). At an overpotential of 240 mV, the catalyst current density remains stable at 20 mA cm^{-2} for 100 h. This exceptional durability shows promise for practical applications of the catalysts over the long term.

To illustrate the relative enhancement of the catalytic activity for TiN NWs, electrochemical impedance spectroscopy (EIS) was further carried out at various HER overpotentials, as shown in the Nyquist plots in Figure 4a. Experimental data were fitted using an equivalent circuit consisting of a resistor (R_s) in series with a parallel combinations of a resistor (R_{ct}) and a constant phase element (CPE), in which R_s represents the ohmic resistance arising from the electrolyte and all contacts, the R_{ct}-CPE reflects the charge transfer resistance (R_{ct}) at the interface between the TiN NWs and the electrolyte (Figure S3).[35, 36] R_{ct} of the TiN NWs electrode as a function of the overpotential applied is plotted in Figure 4b, in which it is clearly seen that R_{ct} is potential-dependent. The Tafel plot derived from the plot of overpotential versus log (R_{ct}^{-1}) (Figure 4b, inset) is 55.7 mV dec^{-1}, which is in accordance with the Tafel slope derived from the polarization curves (Figure 3b). It

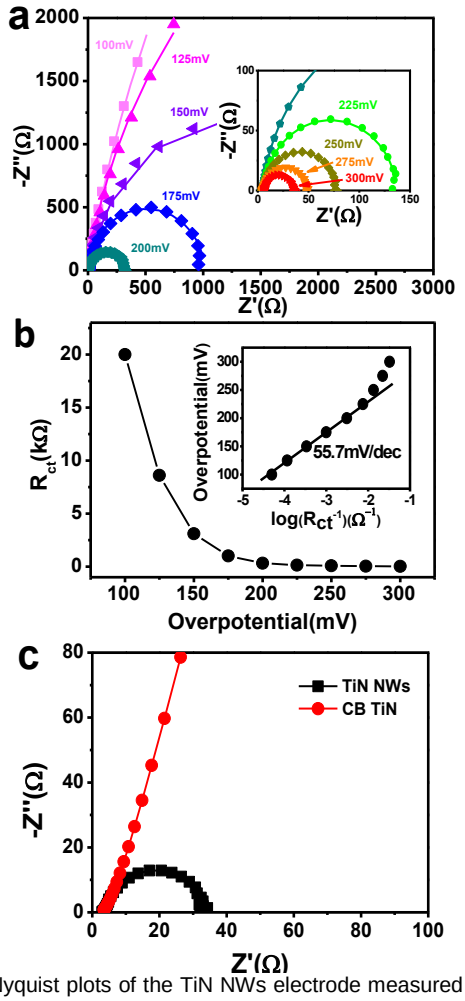

Fig.4 (a) Nyquist plots of the TiN NWs electrode measured at various overpotentials in the frequency range of 10000–0.01 Hz. Scatters: experimental data; line: fitting curves. (b) Dependence of the charge-transfer resistance (Rct) on the overpotential. Inset: overpotential versus log(Rct). (c)Nyquist plots of the TiN NWs electrode and CB TiN electrode measured at overpotential of 0.3 V.

is generally accepted that a smaller Rct gives rise to faster charge transfer kinetics. The TiN NWs electrode displays a smaller Rct than that of CB TiN (Figure 4c), which reveals that TiN NWs afford faster electron transfer rate than that of CB TiN, contributing to the superior kinetics of the HER.

Conclusions

In summary, the ultralong single-crystalline TiN nanowires have been successfully synthesized by a novel CVD method and their electrochemical performance for HER was studied. The as prepared TiN NWs exhibited superior HER performance, with low onset potential of 92 mV, small Tafel slope of 54 mV dec^{-1} and superior electrochemical stability, which is far better than that of commercial bulk TiN. Our work confirms that the TiN NWs is a promising non-noble metal HER catalyst, and also possible to be extended its applications in other fields.

Acknowledgements

This work was supported by the Major International (Regional) Joint Research Project (51210002) , the National Basic Research Program of China (2015CB932304), the Natural Science Foundation of Guangdong province (2015A030312007) and Guangzhou Automobile Group Project (XW6). PKS acknowledge the support from the Danish project of Initiative toward Non-precious Metal Polymer Fuel Cells (4106-000012B).

Notes and references

1 M. Momirlana and T. N. Veziroglu, *Renewable and Sustainable Energy Reviews*, 2002, **6**, 141-179.
2 A. Midilli, M. Ay, I. Dincer and M. A. Rosen, *Renewable and Sustainable Energy Reviews*, 2005, **9**, 273-287.
3 X. Zou and Y. Zhang, *Chemical Society Reviews*, 2015, **44**, 5148-5180.
4 W. F. Chen, J. T. Muckerman and E. Fujita, *Chemical Communications*, 2013, **49**, 8896-8909.
5 J. Shi, Z. Pu, Q. Liu, A. M. Asiri, J. Hu and X. Sun, *Electrochimica Acta*, 2015, **154**, 345-351.
6 J. Xie, S. Li, X. Zhang, J. Zhang, R. Wang, H. Zhang, B. Pan and Y. Xie, *Chemical Science*, 2014, **5**, 4615-4620.
7 W. F. Chen, K. Sasaki, C. Ma, A. I. Frenkel, N. Marinkovic, J. T. Muckerman, Y. Zhu and R. R. Adzic, *Angewandte Chemie*, 2012, **51**, 6131-6135.
8 B. Cao, G. M. Veith, J. C. Neuefeind, R. R. Adzic and P. G. Khalifah, *Journal of the American Chemical Society*, 2013, **135**, 19186-19192.
9 X. Lu, G. Wang, T. Zhai, M. Yu, S. Xie, Y. Ling, C. Liang, Y. Tong and Y. Li, *Nano Letters*, 2012, **12**, 5376-5381.
10 J. Su, N. Lu, J. Zhao, H. Yu, H. Huang, X. Dong and X. Quan, *Journal of Hazardous Materials*, 2012, **231-232**, 105-113.
11 C. Xia, Y. Xie, H. Du and W. Wang, *Journal of Nanoparticle Research*, 2015, **17**, DOI: 10.1007/s11051-014-2855-7.
12 Y. Hu, K. Huo, Y. Ma, Y. Lü, J. Xu, Z. Hu and Y. Chen, *Journal of Nanoscience and Nanotechnology*, 2007, **7**, 2922-2926.
13 M.-S. Balogun, M. Yu, C. Li, T. Zhai, Y. Liu, X. Lu and Y. Tong, *Journal of Materials Chemistry A*, 2014, **2**, 10825-10829.
14 D. Sun, J. Lang, X. Yan, L. Hu and Q. Xue, *Journal of Solid State Chemistry*, 2011, **184**, 1333-1338.
15 M. Luo, J. Gao, X. Zhang, G. Hou, J. Yang, D. Ouyang, H. Wang and Z. Jin, *Journal of Materials Science*, 2007, **42**, 3761-3766.
16 J. Zhu and P. K. Shen, *RSC Advances*, 2013, **3**, 14686-14690.
17 R. S. Wagner and W. C. Ellis, *Applied Physics Letters*, 1964, **4**, 89-90.
18 A. Umar, S. H. Kim, Y. S. Lee, K. S. Nahm and Y. B. Hahn, *Journal of Crystal Growth*, 2005, **282**, 131-136.
19 M. Kakati, B. Bora, S. Sarma, B. J. Saikia, T. Shripathi, U. Deshpande, A. Dubey, G. Ghosh and A. K. Das, *Vacuum*, 2008, **82**, 833-841.
20 S. Kaskel, K. Schlichte, G. Chaplais and M. Khanna, *Journal of Materials Chemistry*, 2003, **13**, 1496-1499.
21 P. Patsalas and S. Logothetidis, *Journal of Applied Physics*, 2001, **90**, 4725-4734.
22 M. A. Bakera, S. J. Greaves, E. Wendler and V. Fox, *Thin Solid Film*, 2000, **377-378**, 473-477.
23 P. Y. Jouan, M. C. Peignon, C. Cardinaud and G. Lempérière, *Applied Surface Science*, 1993, **68**, 595-603.
24 J. Yang, D. Voiry, S. J. Ahn, D. Kang, A. Y. Kim, M. Chhowalla and H. S. Shin, *Angewandte Chemie*, 2013, **52**, 13751-13754.
25 H. Wang, D. Kong, P. Johanes, J. J. Cha, G. Zheng, K. Yan, N. Liu and Y. Cui, *Nano Letters*, 2013, **13**, 3426-3433.
26 M. A. Lukowski, A. S. Daniel, F. Meng, A. Forticaux, L. Li and S. Jin, *Journal of the American Chemical Society*, 2013, **135**, 10274-10277.
27 E. J. Popczun, J. R. McKone, C. G. Read, A. J. Biacchi, A. M. Wiltrout, N. S. Lewis and R. E. Schaak, *Journal of the American Chemical Society*, 2013, **135**, 9267-9270.
28 D. Kong, H. Wang, Z. Lu and Y. Cui, *Journal of the American Chemical Society*, 2014, **136**, 4897-4900.
29 K. C. Neyerlin, W. Gu, J. Jorne and H. A. Gasteiger, *Journal of The Electrochemical Society*, 2007, **154**, B631-B635.
30 Z. Zeng, C. Tan, X. Huang, S. Bao and H. Zhang, *Energy & Environmental Science*, 2014, **7**, 797-803.
31 B. E. Conway and B. V. Tilak, *Electrochimica Acta*, 2002, **47**, 3571-3594.
32 D. Kong, H. Wang, Z. Lu and Y. Cui, *Journal of the American Chemical Society*, 2014, **136**, 4897−4900.
33 J. O. M. Bockris and E. C. Potter, *Journal of the Electrochemical Society*, 1952, **99**, 169-186.
34 M. Jafarian, O. Azizi, F. Gobal and M. G. Mahjani, *International Journal of Hydrogen Energy*, 2007, **32**, 1686-1693.
35 J. Kubisztal, A. Budniok and A. Lasia, *International Journal of Hydrogen Energy*, 2007, **32**, 1211-1218.
36 L. Liao, S. Wang, J. Xiao, X. Bian, Y. Zhang, M. D. Scanlon, X. Hu, Y. Tang, B. Liu and H. H. Girault, *Energy & Environmental Science*, 2014, **7**, 387-392.